Electronic Supplementary Material (ESI) for Green Chemistry.

Supporting Information

Electrosynthesis of New Quinone Sulfonimide Derivatives using Conventional Batch and a New Electrolyte Free Flow Cells

Shima Momeni, and Davood Nematollahi*

Faculty of Chemistry, Bu-Ali Sina University, Hamedan, Zip Code 65178-38683. Iran

Table of Contents:

Design and characteristics of electrochemical flow-cell

Figure **S1** shows schematic illustration of the electrochemical flow cell. As can be seen, the cell is constructed from eight parallel rectangular plates. It is strongly compressed between two 6 mm thickness iron plates (**1** and **11** in Fig. **S1**) using then edge bolts (12 and 13), as long as the more equally distribute pressure across the plates is sufficient to achieve efficient sealing of the cell and avoid the leakage of the stack. The anode electrode is a carbon plate (**8**) with thickness of 6.0 mm, the cathode is stainless steel (**3**) (thickness 2.0 mm, grade 316). It also incorporates two fluid inlet/outlet holes which a steel tubing (6mm diameter, and 25mm length) have welded to the plate (**5**). As well as, insulating Plexiglass plate (**2** and **10)** with thickness of 2.0 mm is placed below the top and bottom plates in order to electrically insulate iron sheets from the electrodes and also a copper plate (**9**) (1.0 mm thickness) is placed at the back of the carbon electrode to improve the potential distribution along the electrolyte channel. The anode and cathode plates separated by the polytetrafluoroethylene (PTFE) gasket/spacer plate with 1.0 mm thickness. the flow channels within the spacer were cut by laser (Fiber laser cutting), providing the exact shape required. In the present work, we have described "snaking" channel pattern (**7**). The channel is 190.0 mm in length and 6.0 mm in width with an interelectrode gap of 1.0 mm. Such a design provides a total channel path-length of 156.2 cm, a cell volume of 9.93 cm^3 and giving an active electrode surface of 93.3 cm^2. It should be mentioned that what distinguishes this cell design from other is that, in most of the cell design which has previously performed, the solution flow channel was created by machining the grooves into at least one of the electrodes and a gasket/spacer must cut with the exact matching pattern to the groove, so that it fitted into the groove. However, in the present cell, there is no machined groove into the electrodes and only the thickness of the spacer controls the interelectrode gap. Thus, the gap can be easily optimized as required with the thickness of spacer

in order to find an optimum interelectrode gap for allowing the cell working without intentionally added supporting electrolyte. The optimum narrow interelectrode gap was 1 mm in this work. As mentioned in literature,[1] one of the challenges in bulk electrolysis is when a nonaqueous solvent with lower dielectric constants are used and therefore, lower conductivities lead to high cell resistances. To overcome this problem, more quantity of supporting electrolyte is needed that is costly and uneconomical. One of the most important advantages of our reactor is performing in the absence of supporting electrolyte due to the low interelectrode gaps. In all of our experiments, even in the high current densities the cell voltage was low (0.5–4.0 V).

1. M. B. Plutschack, B. u. Pieber, K. Gilmore, P. H. Seeberger, *Chem. Rev.* **2017**, *117*, 11796-11893

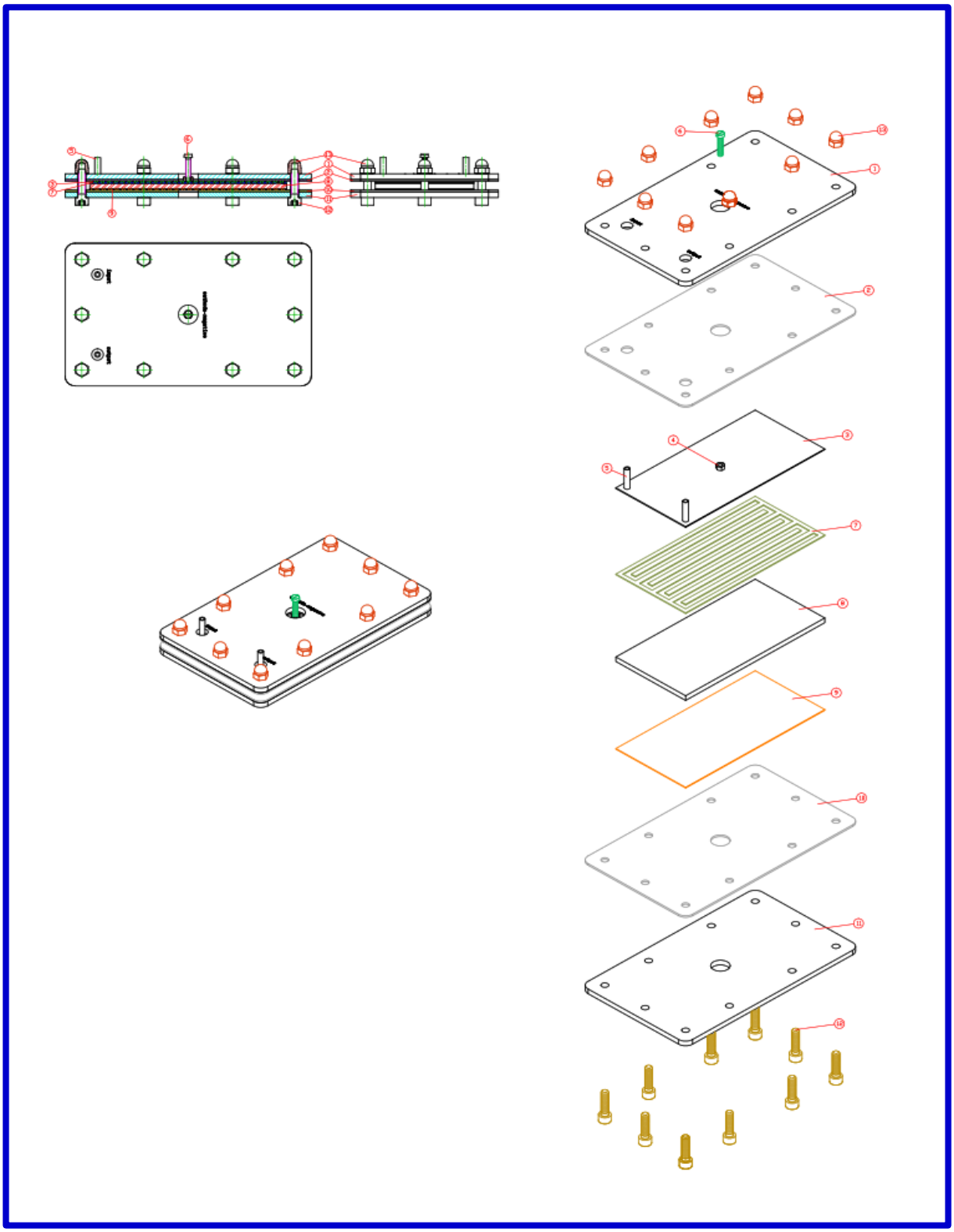

Figure S1. Schematic illustration of the flow reactor.

Calculations of yield and conversion

The yield of product (**QSI**) is calculated as below:

% Yield= Actual mole of **QSI**/ theoretically mole of **QSI** ×100

The conversion of **APE** in continuous flow reactor has been estimated based on the comparison of I_{pA1} before entering the cell with the I_{pA1} after leaving the flow cell. For instance, the cyclic voltammograms of **APE** in the presence of **ASA1-3**, before entering and after leaving the flow cell in a single pass at optimum conditions, have been shown in Figures 8, S2 and S3.

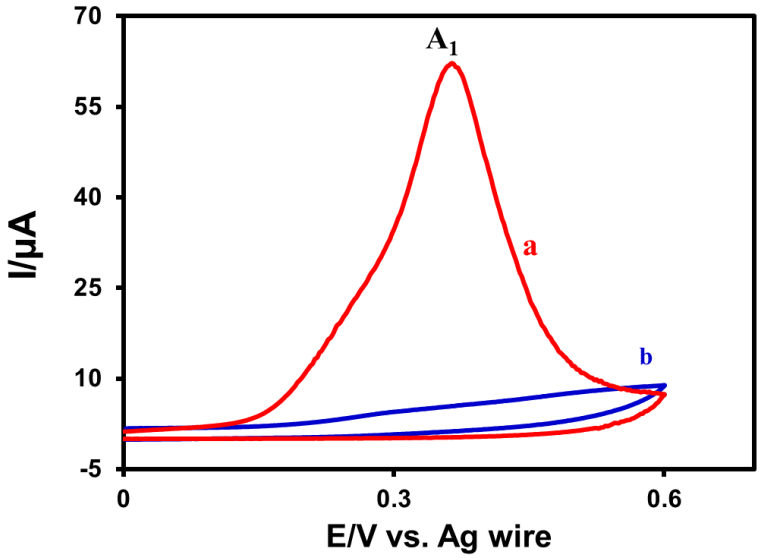

Figure S2. Cyclic voltammograms of **APE** in the presence of **ASA2**. (a) before entering the flow cell. (b) after leaving the flow cell. Solvent: water/ethanol mixture (20/80 v/v). Scan rate: 0.1 V s^{-1}. Flow rate: 0.5 mL min^{-1}. Current density: 1.88 mA cm^{-2}.

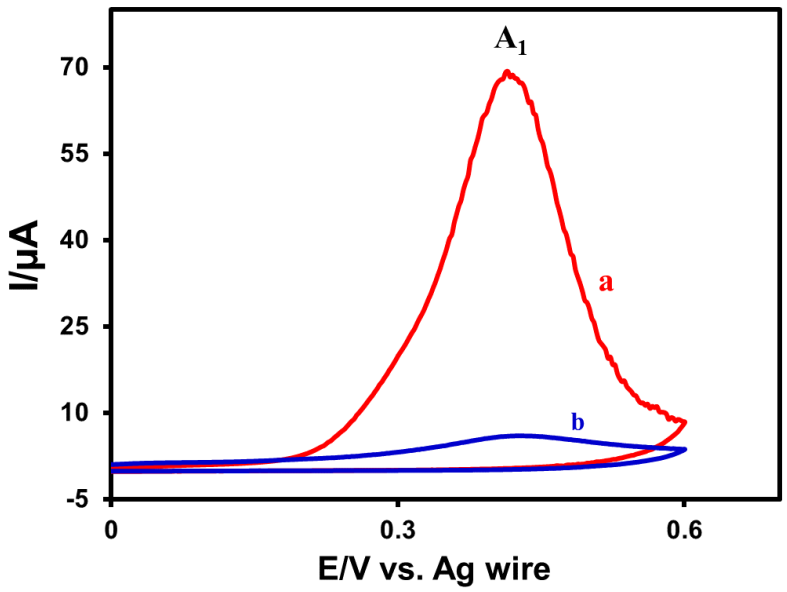

Figure S3. Cyclic voltammograms of **APE** in the presence of **ASA3**. (a) before entering the flow cell. (b) after leaving the flow cell. Solvent: water/ethanol mixture (20/80 v/v). Scan rate: 0.1 V s^{-1}. Flow rate: 0.5 mL min^{-1}. Current density: 1.88 mA cm^{-2}.

The effect of potential scan rate

Figure **S2** displays the normalized CVs of **APE** at diff erent scan rates. The normalization was carried out by dividing the current by the square root of the potential scan rate ($I/v^{1/2}$).

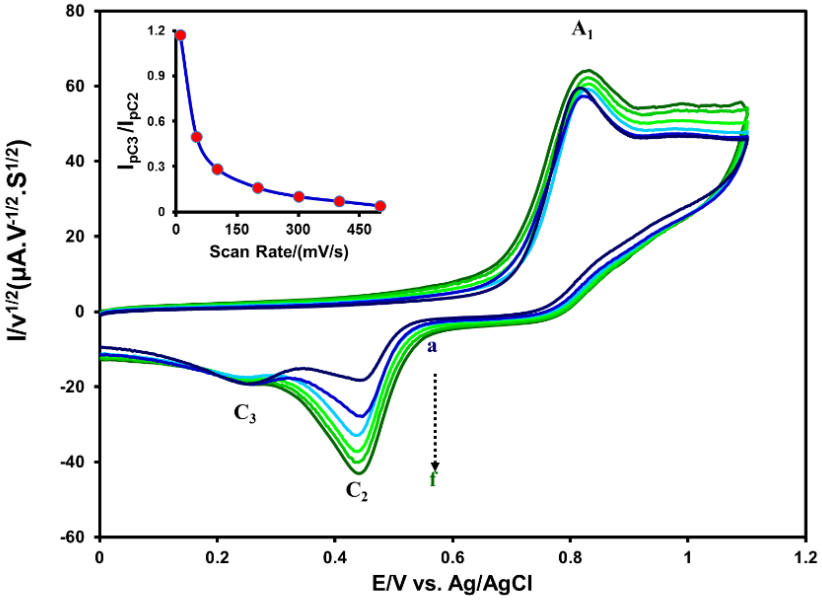

Figure S4. Normalized voltammograms of **APE** (1.0 mM) at a glassy carbon electrode in 0.1 M $HClO_4$ at diff erent scan rates. Scan rates from (a) to (f) are 50, 100, 200, 300, 400 and 500 mV s^{-1}. Inset: variation of peak current ratio I_{pC3}/I_{pC2}. versus scan rate. T = 25 ± 1◦C.

Cyclic voltammogram of APE in the presence of ASA3

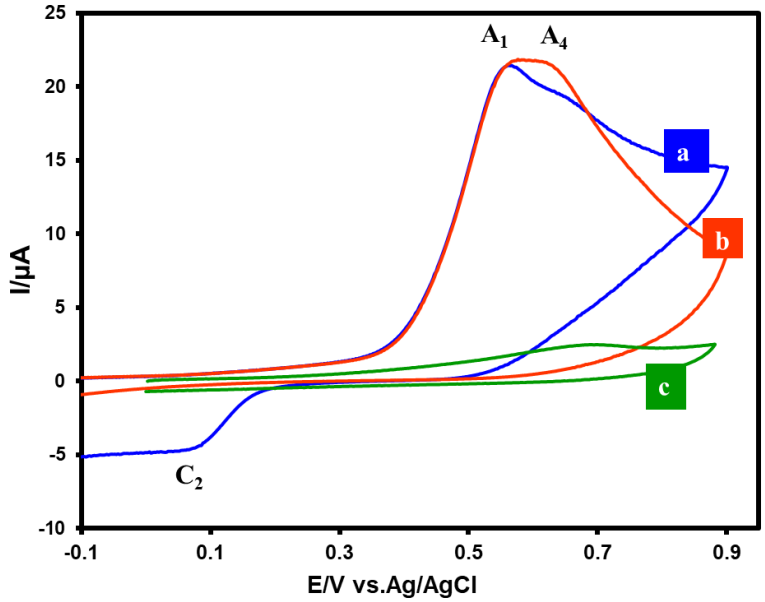

Figure S5. Cyclic voltammograms of **APE** (1.0 mM): (a) in the absence, (b) in the presence of **ASA3** (1.0 mM). (c) Cyclic voltammogram of **ASA3** (1.0 mM). Solvent: water (acetate buffer, *c* = 0.2 M, pH = 5.0)/ethanol mixture (70/30 v/v). Scan rate: 0.1 V s^{-1}. Working electrode: glassy carbon electrode. Temperature = 25 ± 1 ˚C.

Cyclic voltammogram of APE in the presence of ASA2

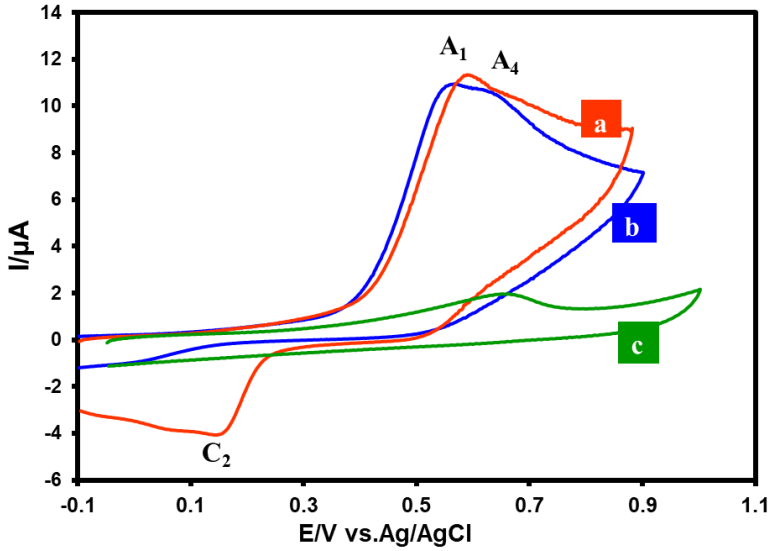

Figure S6. Cyclic voltammograms of **APE** (1.0 mM): (a) in the absence, (b) in the presence of **ASA2** (1.0 mM). (c) Cyclic voltammogram of **ASA2** (1.0 mM). Solvent: water (acetate buffer, *c* = 0.2 M, pH = 5.0)/ethanol mixture (70/30 v/v). Scan rate: 0.1 V s^{-1}. Working electrode: glassy carbon electrode. Temperature = 25 ± 1 ˚C.

Cyclic voltammograms of APE in the presence of ASA3 during electrolysis

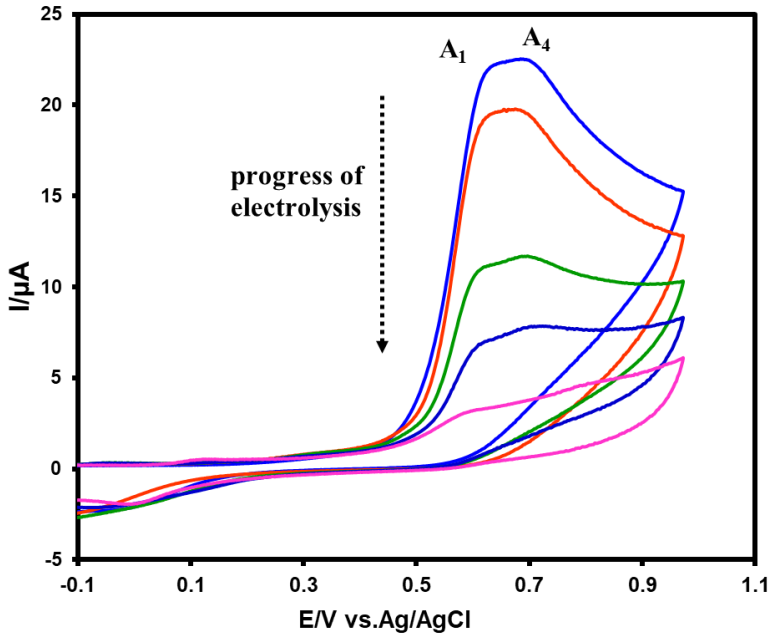

Figure S7. Cyclic voltammograms of **APE** (0.15 mmol) in the presence of **ASA3** (0.75 mmol) during controlled-potential electrolysis. Solvent: water (acetate buffer, c = 0.2 M, pH = 5.0)/ethanol mixture (70/30 v/v). E_{app} = +0.65 V vs. Ag/AgCl. Scan rate: 0.1 V s^{-1}. Working electrode: glassy carbon electrode. Temperature = 25 ± 1 ˚C.

Cyclic voltammograms of APE in the presence of ASA2 during electrolysis

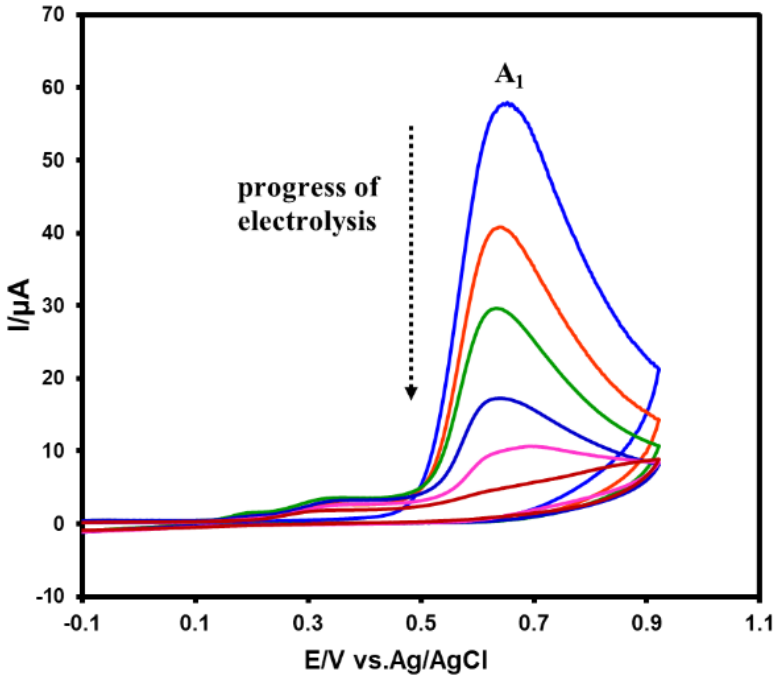

Figure S8. Cyclic voltammograms of **APE** (0.25 mmol) in the presence of **ASA2** (1.0 mmol) during controlled-potential electrolysis. Solvent: water (acetate buffer, c = 0.2 M, pH = 5.0)/ethanol mixture (70/30 v/v). E_{app} = +0.65 V vs. Ag/AgCl. Scan rate: 0.1 V s^{-1}. Working electrode: glassy carbon electrode. Temperature = 25 ± 1 ˚C.

Characteristic of Products

Compound **QSI1** *($C_{20}H_{17}NO_5S_2$)*

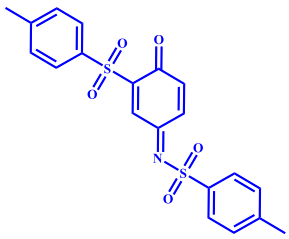

M.p: 122-123 ^{o}C.^{1}H NMR (400 MHz, DMSO-d_6) δ 2.48 (s, 3H), 2.59 (s, 3H), 7.31 (s, 1H), 7.45 (d, J = 8.2 Hz, 2H), 7.64 (d, J = 8.2 Hz, 3H), 7.75 – 7.80 (m, 5H).^{13}C NMR (101 MHz) δ 165.9, 153.7, 145.2, 142.5, 139.0, 138.0, 135.9, 130.1, 129.9, 129.3, 128.7, 128.0, 127.8, 108.6, 21.2, 21.0. IR (KBr) ν =3067 (Weak, Aromatic C-H), 2923 (Weak, Aliphatic C-H), 1596 (Strong, conjugated C=O), 1501 (medium, C=C), 1493 (medium, C-H bending), 1377 (strong, S=O), 1168 (strong, S=O), 1140, 1084, 813, 663, 548 cm^{-1}. MS (EI, 70 eV, m/z) (relative intensity): 417 (M+2, 24), 416 (M+1, 34), 321 (11), 283 (27), 261 (49), 251 (53), 195 (15), 155(59), 107 (13), 91 (100), 43 (30)

Compound **QSI2** *($C_{18}H_{13}NO_5S_2$)*

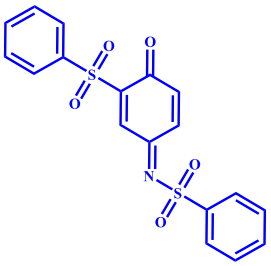

M.p: 129-130 ^{o}C ^{1}H NMR (301 MHz, DMSO-d_6) δ 7.25 (s, 1H), 7.51 – 7.62 (m, 3H), 7.63 – 7.70 (m, 1H), 7.70 – 7.81 (m, 5H), 7.84 (d, J = 7.3 Hz, 2H), 7.90 (t, J = 7.3 Hz, 1H). ^{13}C NMR (76 MHz) δ 166.4, 157.9, 142.2, 139.1, 138.7, 135.1, 132.8, 130.2, 130.1, 129.6, 128.8, 128.3, 128.2, 109.2. IR (KBr) ν =3064 (Weak, Aromatic C-H), 1591 (medium, conjugated C=O), 1499 (strong,

C=C), 1448 (medium, C-H bending), 1379 (strong, S=O), 1172 (strong, S=O), 1140, 1083, 942, 866, 721, 685, 570 cm^{-1} .MS (EI, 70 eV, m/z) (relative intensity): 389 (M+2, 21), 388 (M+1, 36), 248 (2), 224 (10), 180 (5), 141 (16), 125 (17), 109 (21), 77 (100), 51 (42)

Compound **QSI3** *($C_{18}H_{11}Cl_2NO_5S_2$)*

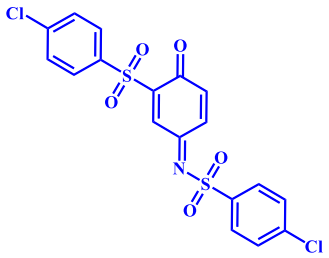

M.p: 149-150 ºC.^{1}H NMR (301 MHz, DMSO-d_6) δ 7.32 (s, 1H), 7.72 (d, J = 8.6 Hz, 2H), 7.75 – 7.87 (m, 2H), 7.89 (d, J = 8.6 Hz, 2H), 7.95 (s, 4H). ^{13}C NMR (76 MHz, DMSO) δ 166.4, 158.1, 140.8, 140.4, 138.6, 138.0, 137.6, 130.5, 130.4, 130.3, 130.2, 129.6, 129.0, 108.9. IR (KBr) ν =3090 (Weak, Aromatic C-H), 1587 (medium, conjugated C=O), 1498 (strong, C=C), 1477 (medium, C-H bending), 1388 (strong, S=O), 1169 (strong, S=O), 1091, 1013, 944, 795, 756 (strong, C-Cl), 617, 564 cm^{-1}. MS (EI, 70 eV, m/z) (relative intensity): 457 (M+2, 9), 456 (M+1, 11), 284 (24), 282 (59), 175 (72), 112 (51), 111 (100), 106 (73), 75 (49), 50 (16),

IR spectrum of QSI1

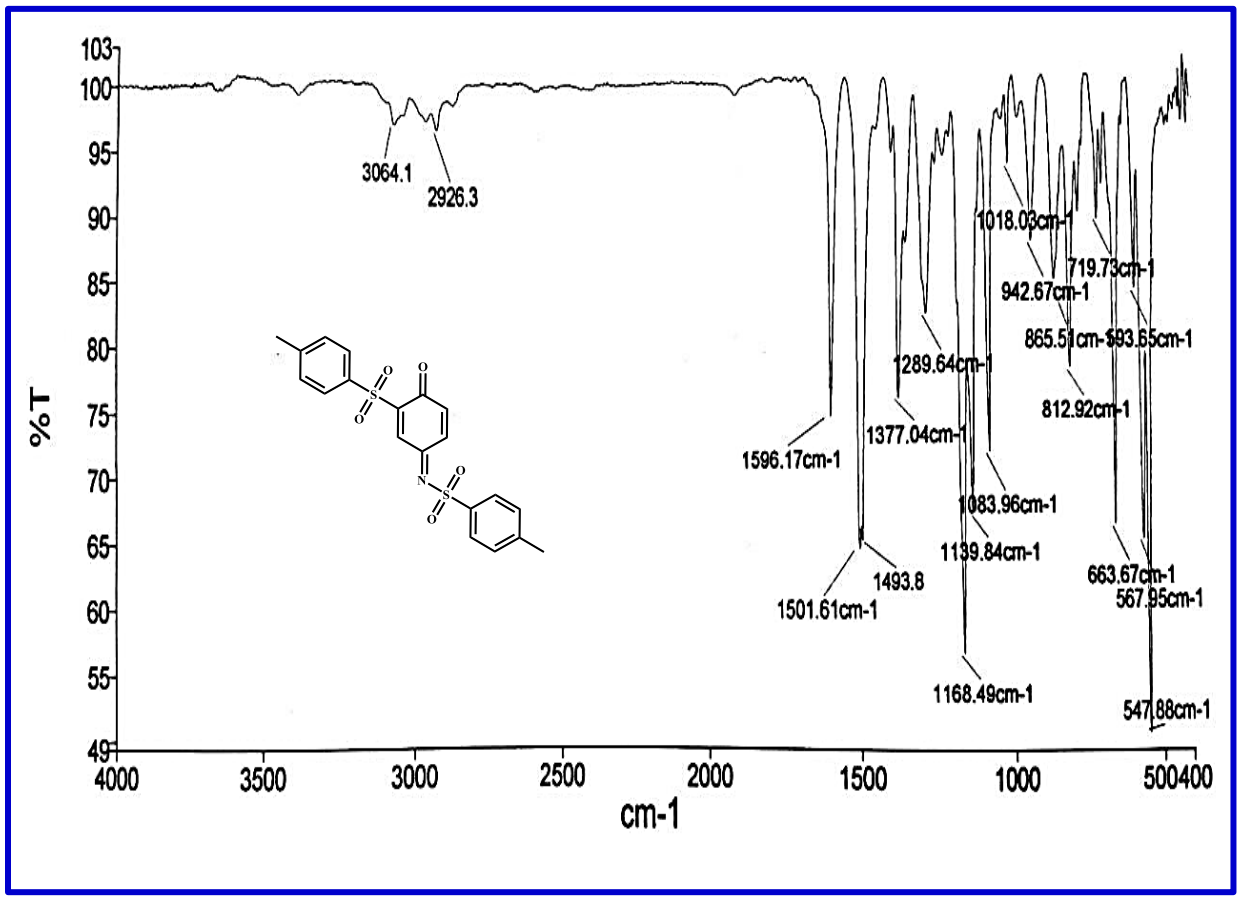

^{1}H NMR spectrum of QSI1

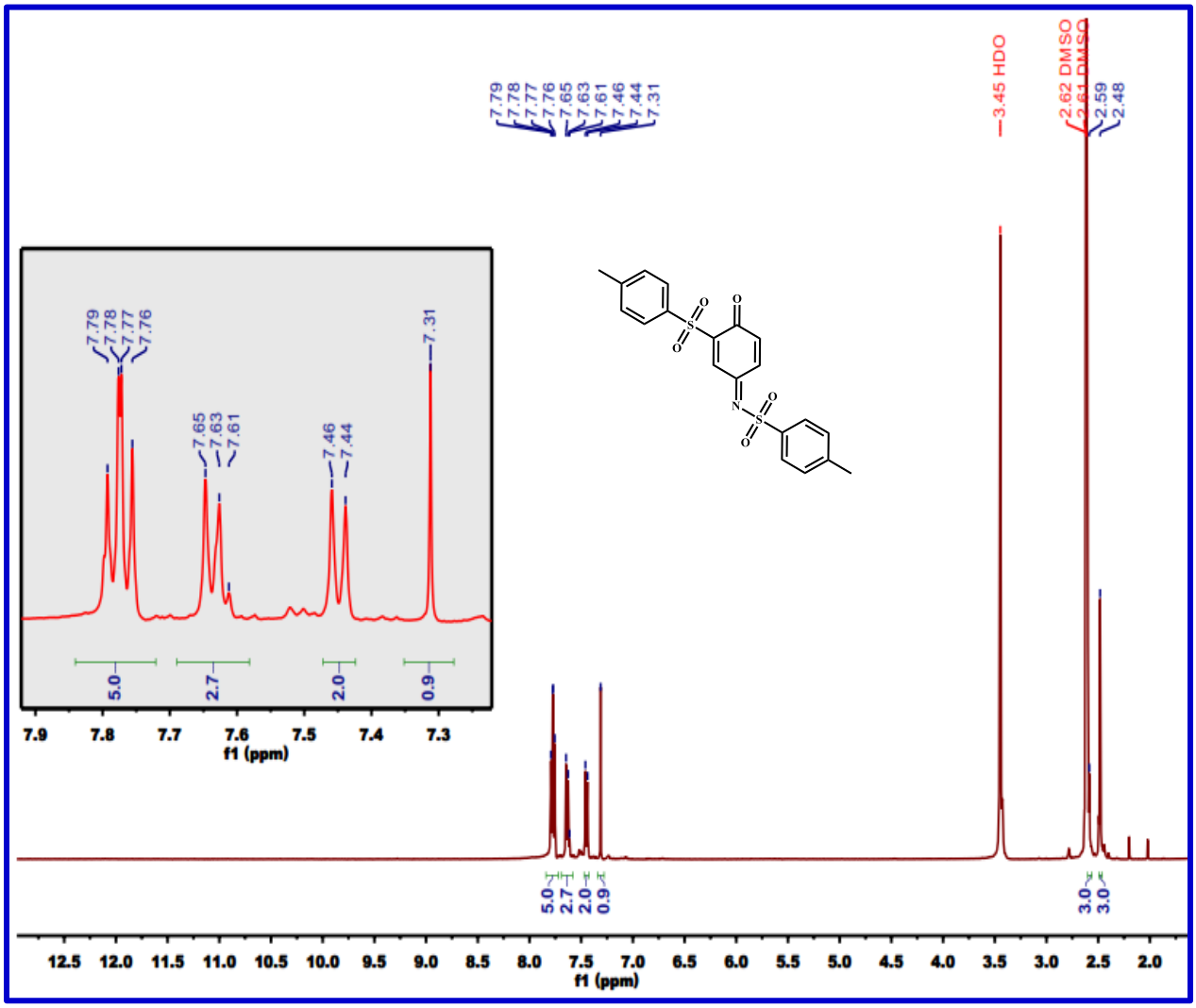

^{1}H NMR spectrum of QSI1 (with D_2O)

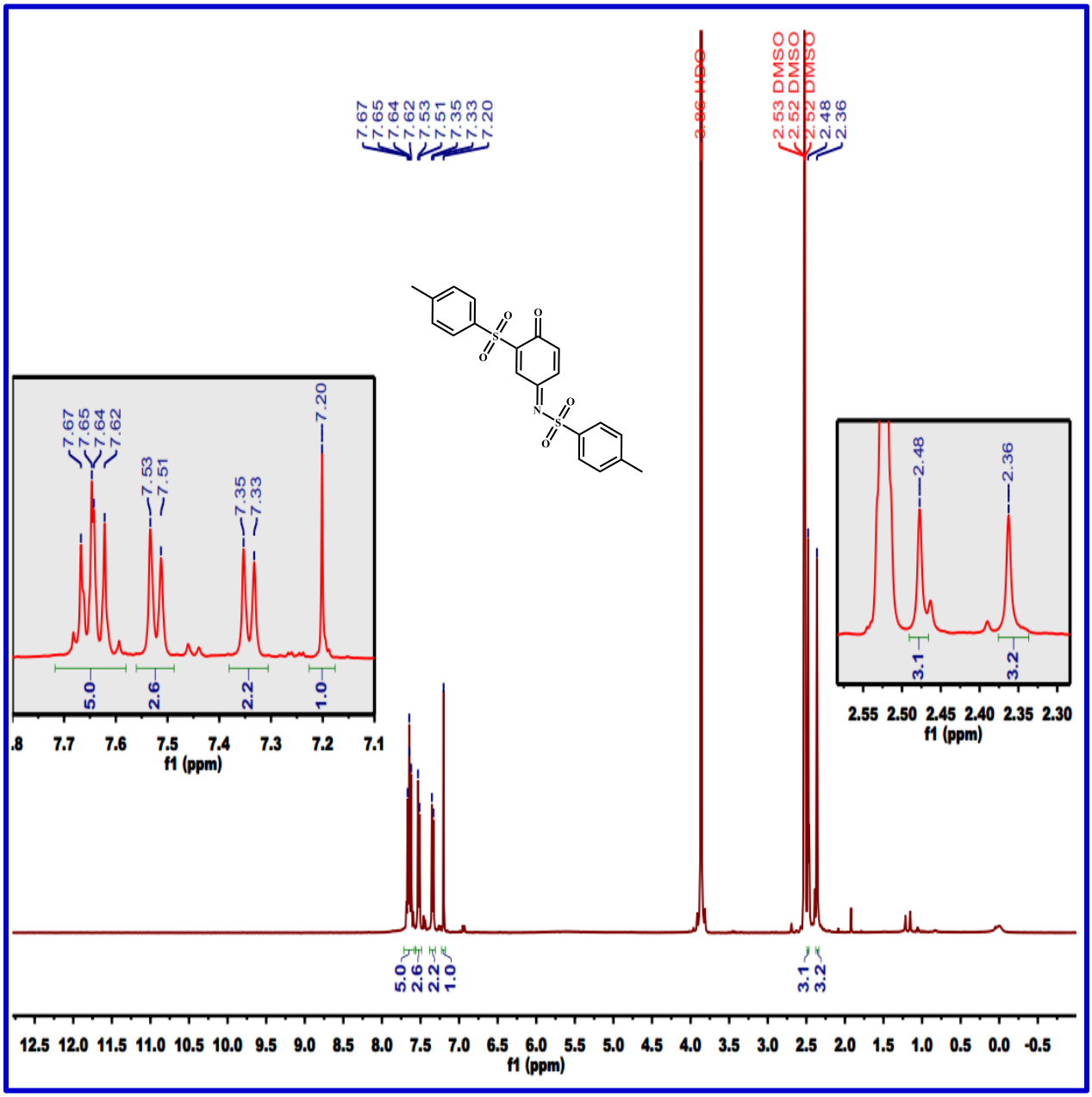

^{13}C NMR spectrum of QSI1

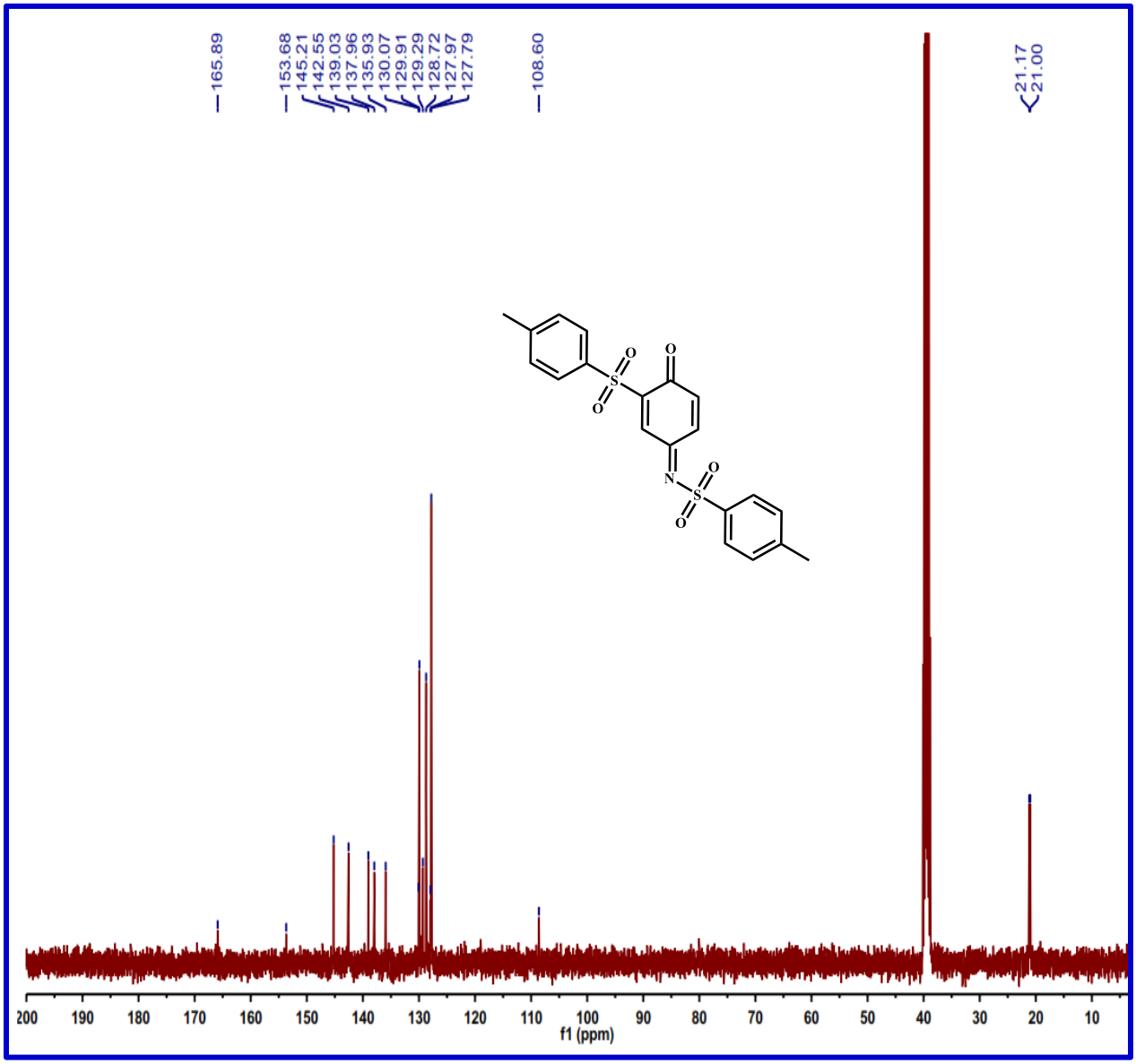

MS spectrum of QSI1

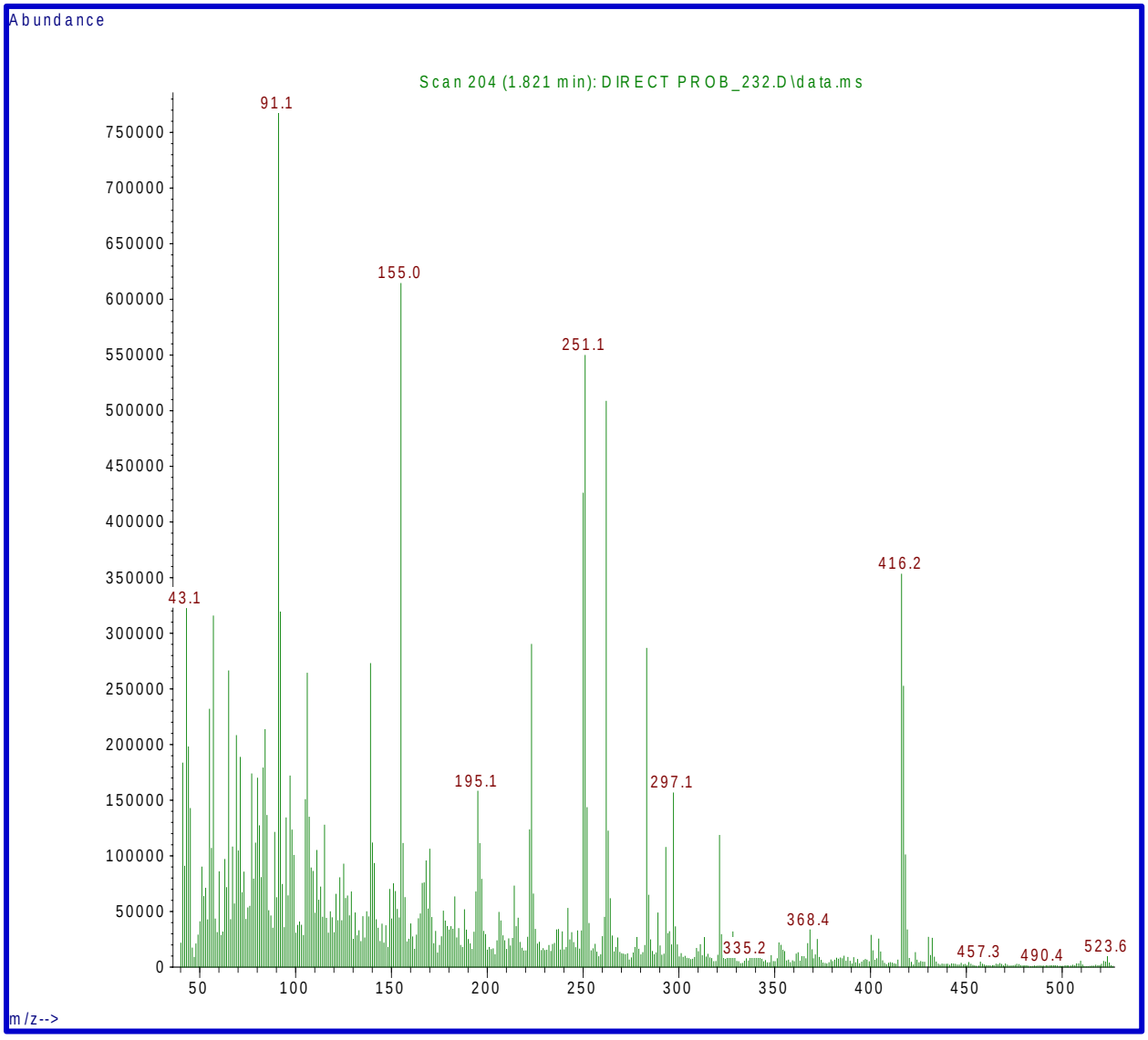

IR spectrum of QSI2

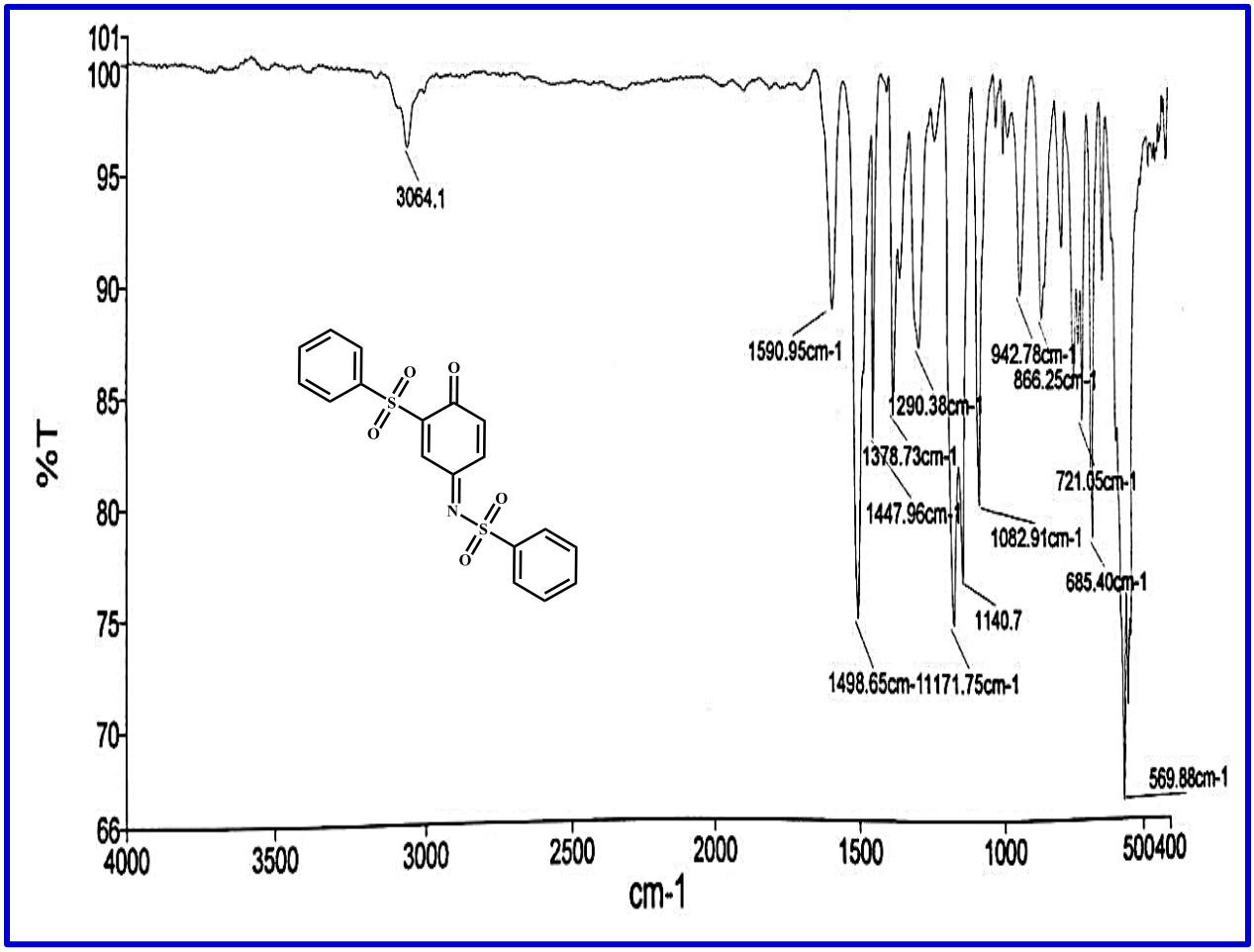

^{1}H NMR spectrum of QSI2

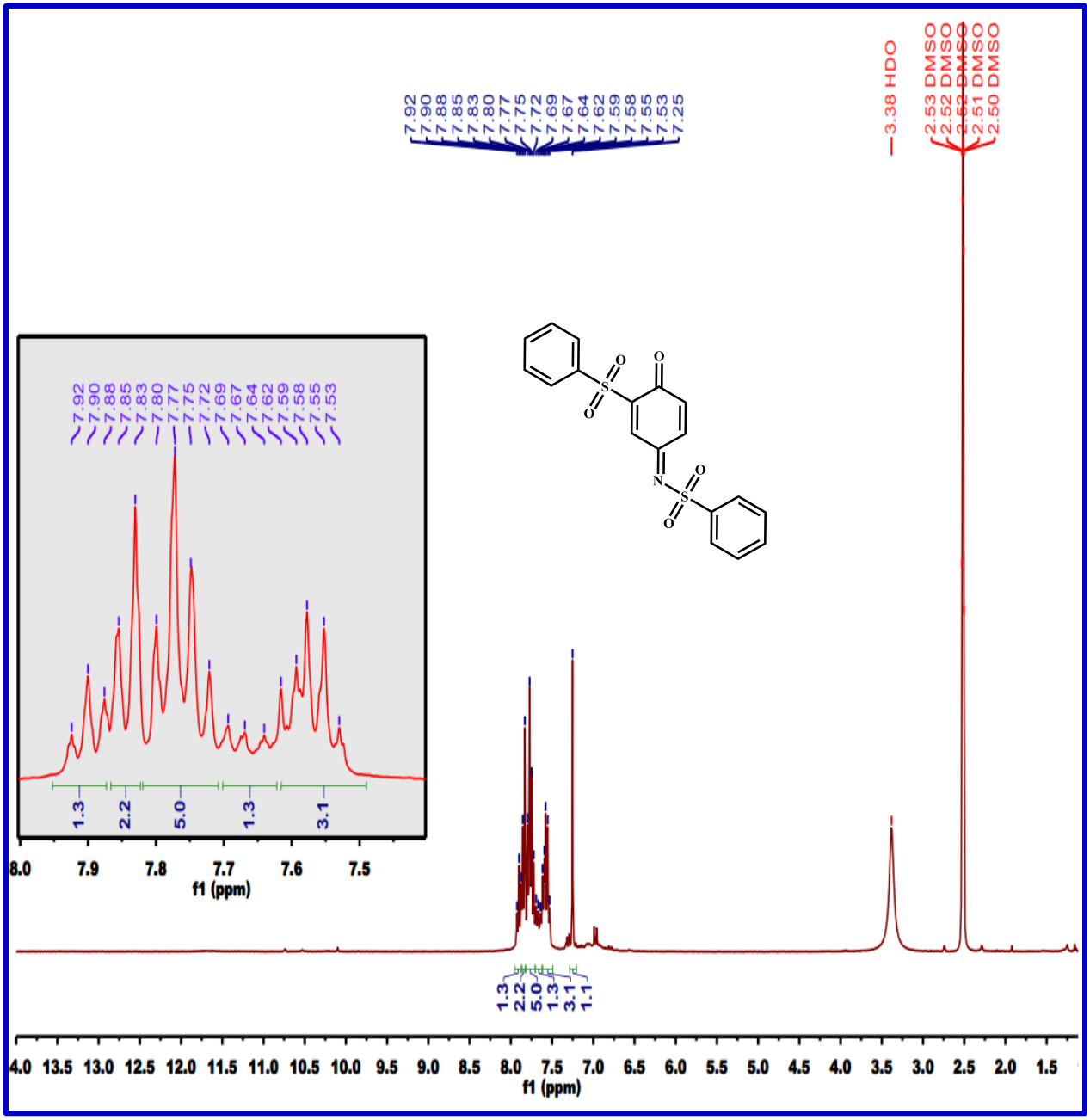

The peaks in the region between 6.5 ppm and 7.4 ppm (except peak, δ = 7.25 ppm) are related to impurities.

^{1}H NMR spectrum of QSI2 (with D_2O)

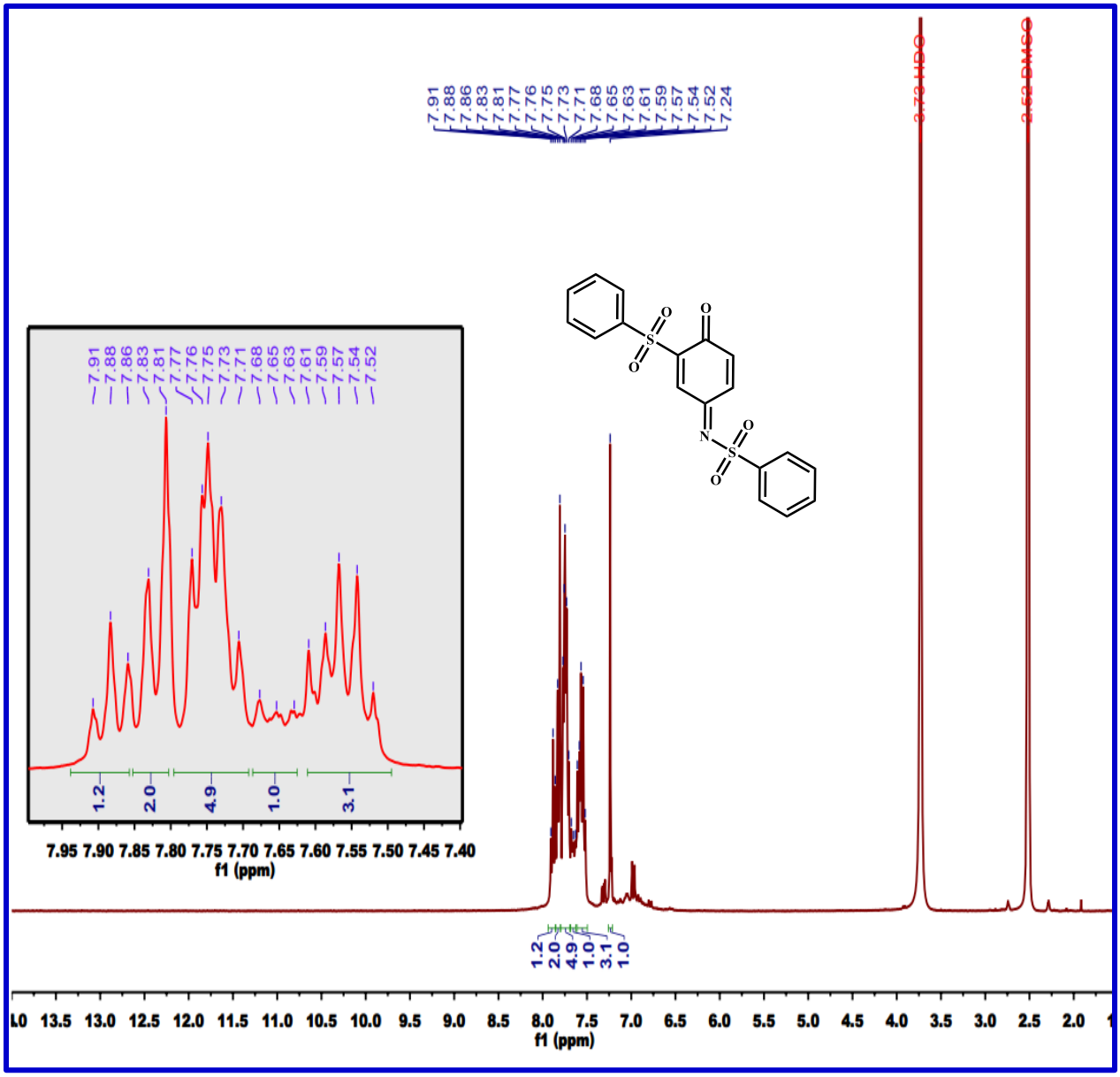

The peaks in the region between 6.5 ppm and 7.4 ppm (except peak, δ = 7.25 ppm) are related to impurities.

^{13}C NMR spectrum of QSI2

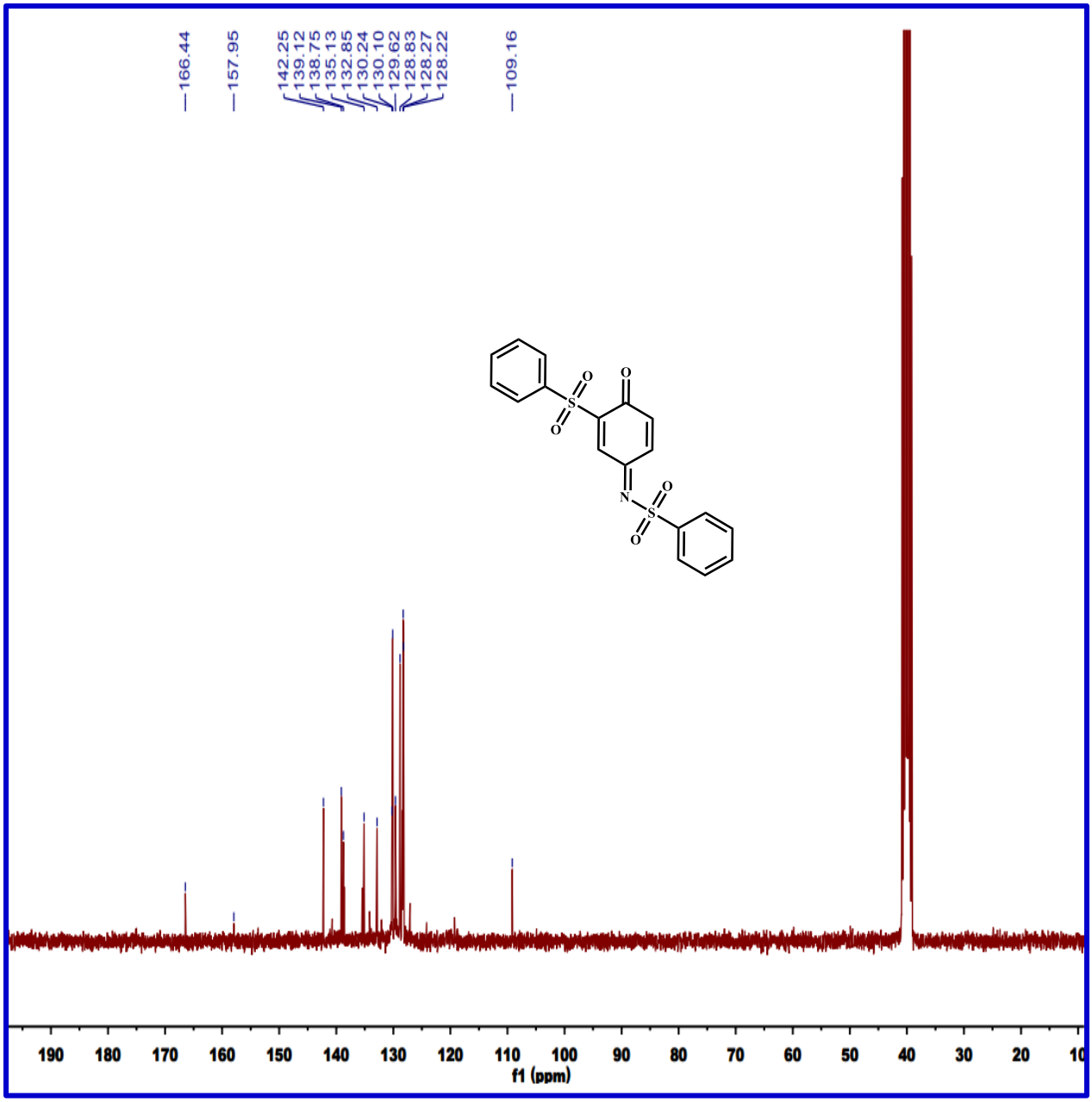

The peaks in δ = 118, 127 and 131 ppm are related to impurities.

MS spectrum of QSI2

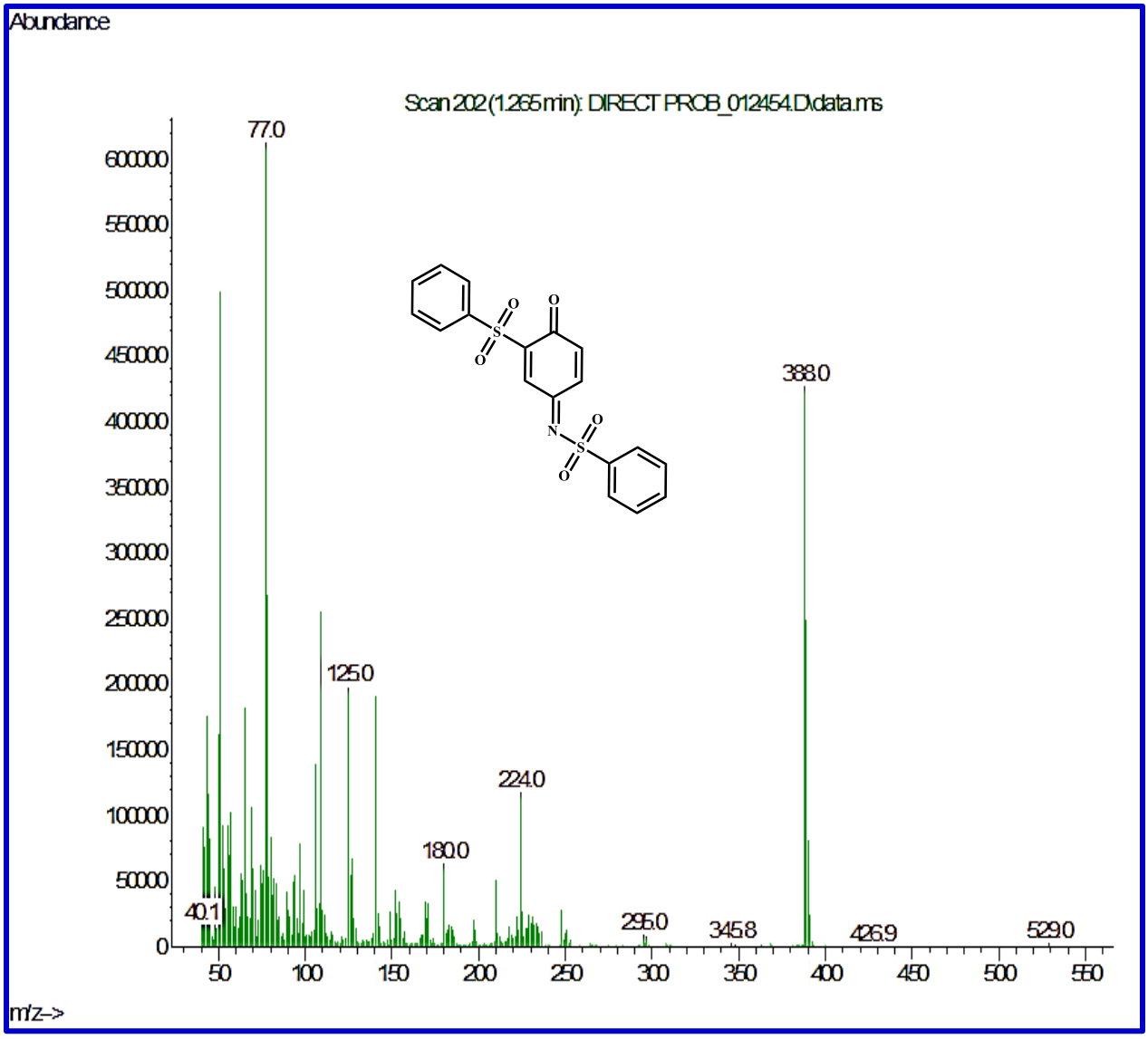

IR spectrum of QSI3

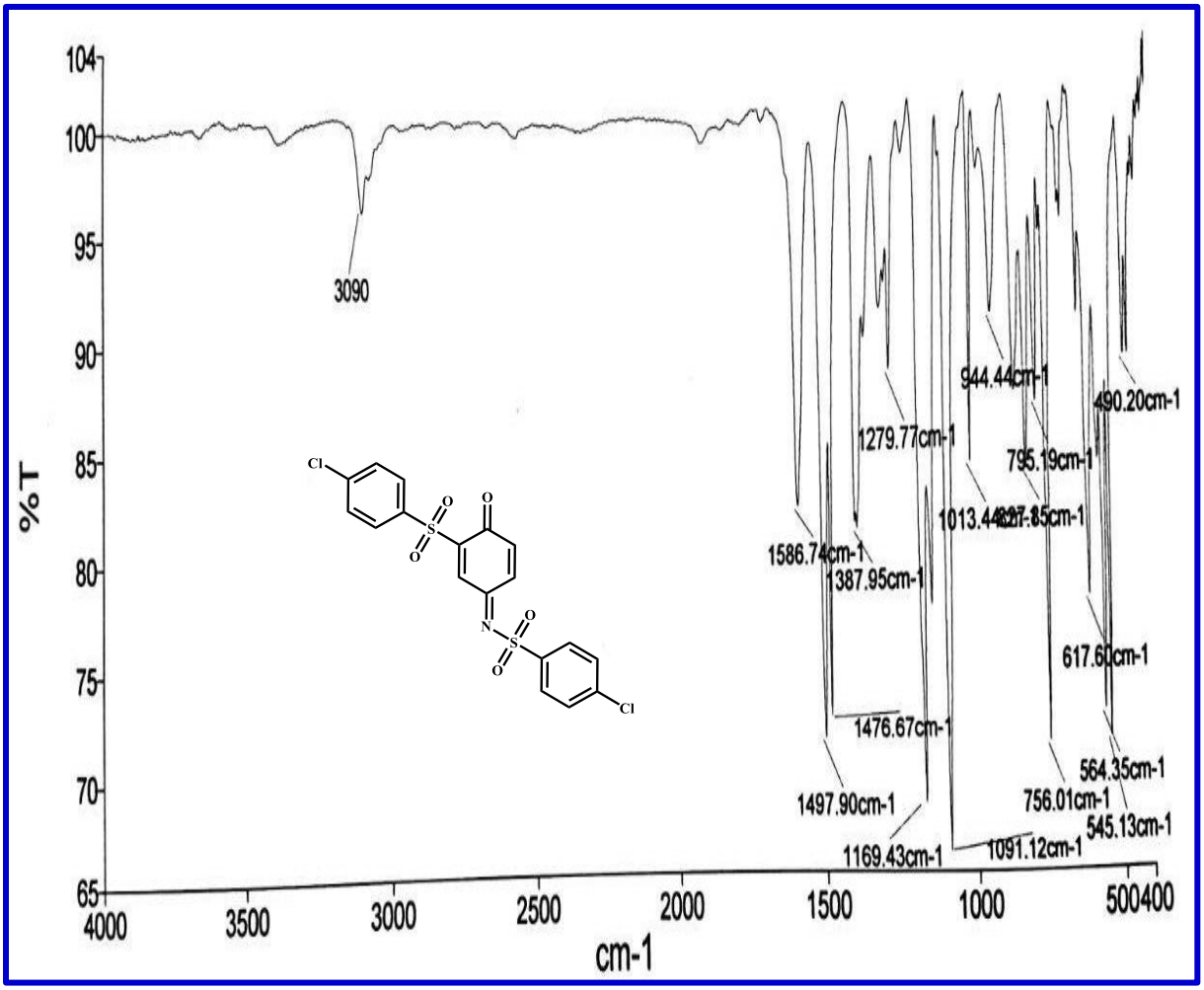

^{1}H NMR spectrum of QSI3

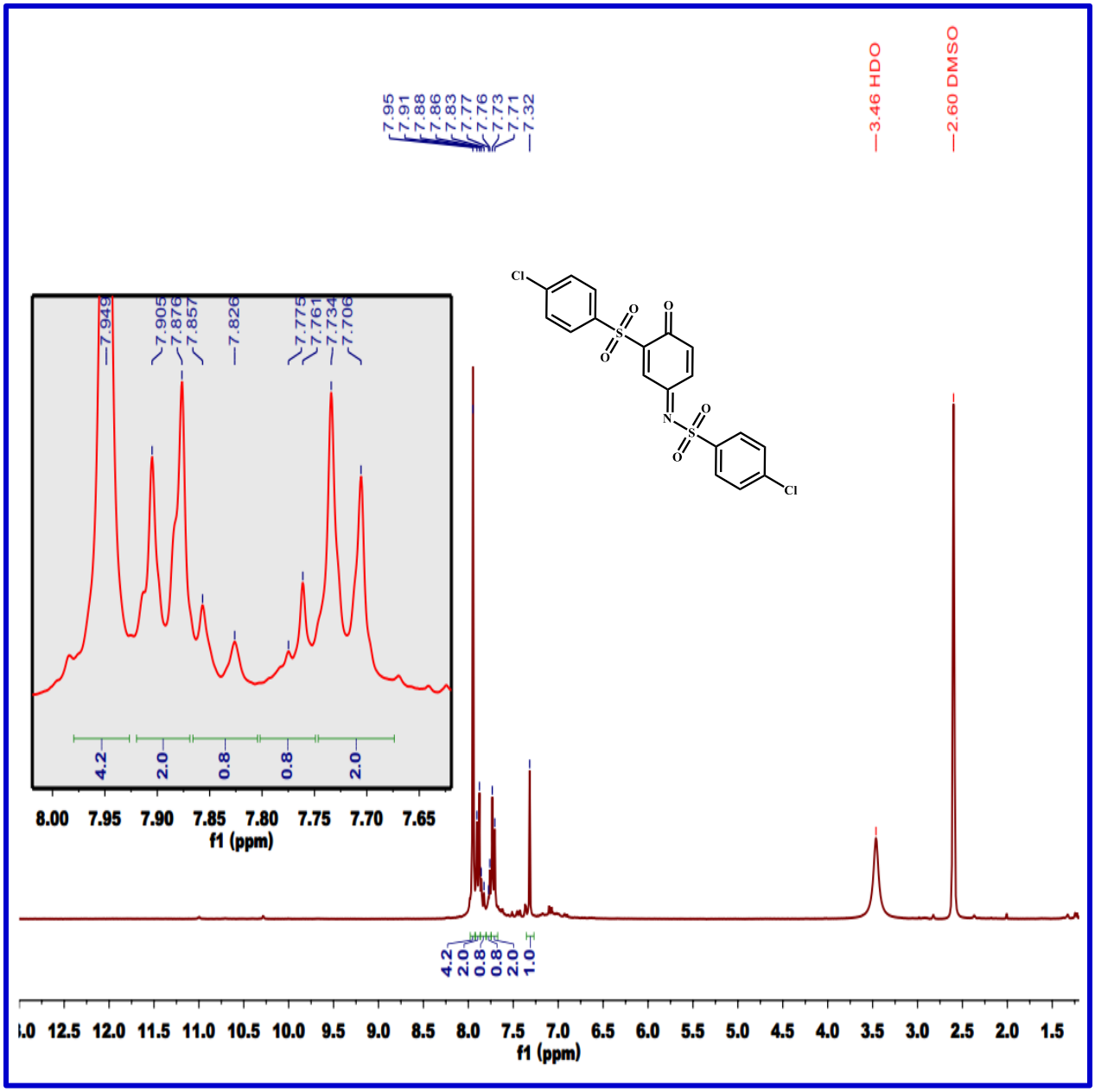

The peaks in the region between 6.5 ppm and 7.5 ppm (except peak, δ = 7.32 ppm) are related to impurities.

^{13}C NMR spectrum of QSI3

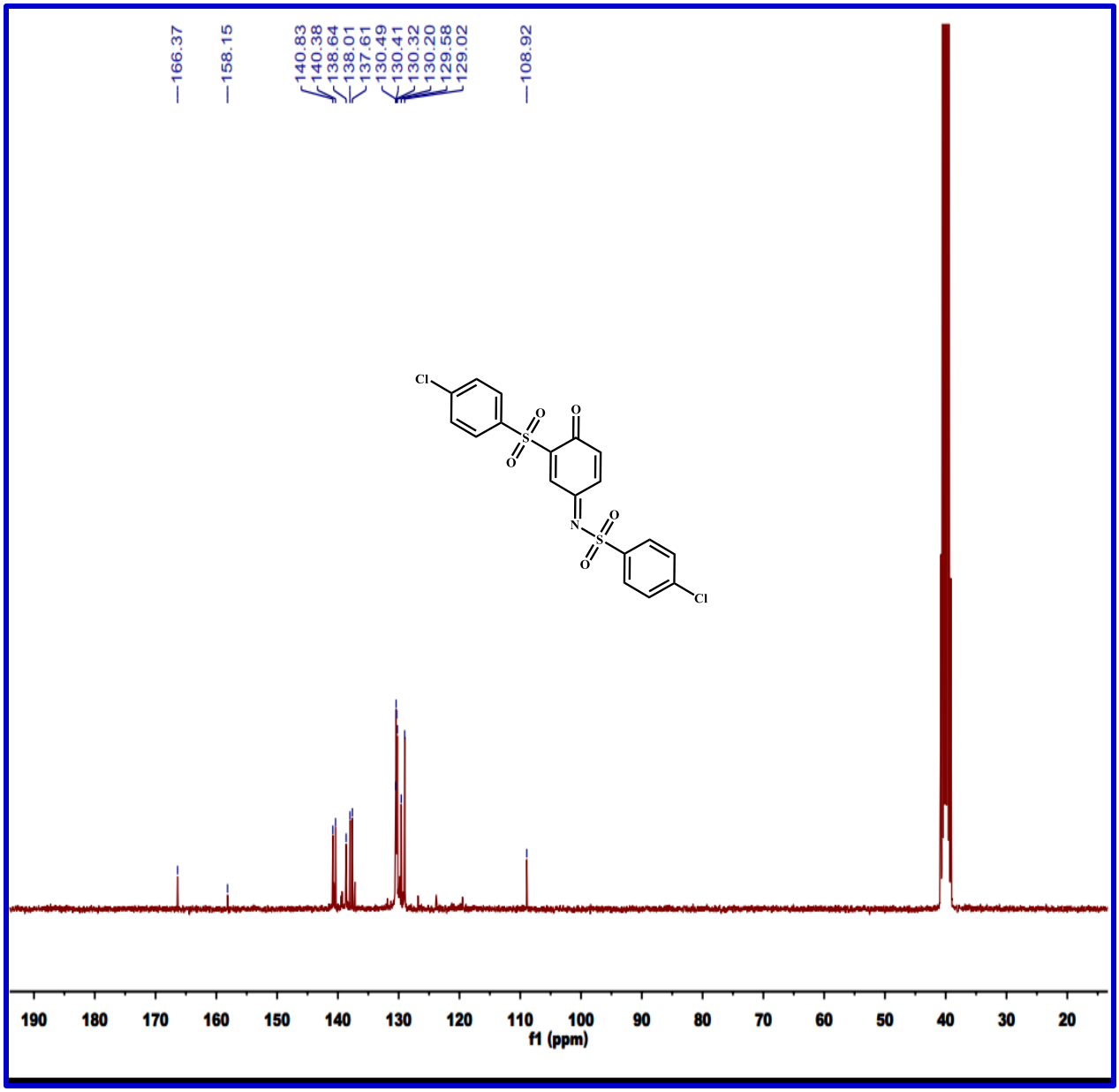

The peaks between 115 and 128 ppm are related to impurities.

MS spectrum of QSI3